

OPEN ACCESS

Communication—Prediction of Thermal Issues for Larger Format 4680 Cylindrical Cells and Their Mitigation with Enhanced Current Collection

To cite this article: T. G. Tranter *et al* 2020 *J. Electrochem. Soc.* **167** 160544

View the [article online](#) for updates and enhancements.



Communication—Prediction of Thermal Issues for Larger Format 4680 Cylindrical Cells and Their Mitigation with Enhanced Current Collection

T. G. Tranter,^{1,3,z} R. Timms,^{2,3} P. R. Shearing,^{1,3} and D. J. L. Brett^{1,3,z}

¹Electrochemical Innovation Lab, Department of Chemical Engineering, University College London, London, WC1E 7JE, United Kingdom

²Mathematical Institute, University of Oxford, Oxford, OX2 6GG, United Kingdom

³The Faraday Institution, Quad One, Becquerel Avenue, Harwell Campus, Didcot, OX11 0RA, United Kingdom

The paper numerically explores the electrochemical and thermal behaviour of a larger format 4680 cylindrical cell recently proposed by Tesla and explains the need to go “tabless.” An idealized spiral geometry is used for 2D simulations with the traditional tab-based current collection method and a new continuous current collection method compared. The new design is found to mitigate the ohmic losses experienced around the “jelly-roll” current collectors which are significant for the traditional tabbed case, thus leading to higher efficiency and capacity and reduced heat production.

© 2020 The Author(s). Published on behalf of The Electrochemical Society by IOP Publishing Limited. This is an open access article distributed under the terms of the Creative Commons Attribution 4.0 License (CC BY, <http://creativecommons.org/licenses/by/4.0/>), which permits unrestricted reuse of the work in any medium, provided the original work is properly cited. [DOI: 10.1149/1945-7111/abd44f]



Manuscript submitted October 20, 2020; revised manuscript received December 3, 2020. Published December 29, 2020.

Supplementary material for this article is available [online](#)

Traditional Li-ion cell designs have their limitations from a thermal management perspective.^{1–4} In particular, the long length of the electrode spiral or “jelly-roll” in cylindrical cells leads to heterogeneity in current distribution and temperature when current collection is performed by tabs at the ends of the roll.⁵ The insulative nature of the components being wrapped around themselves also leads to internal temperature gradients between the core and surface of the battery. Combined, these effects can lead to other non-uniformities in state-of-charge, particle stress and levels of degradation.^{6–12} Introducing additional tabs may alleviate current heterogeneity but can also lead to mechanical stress that can cause accelerated degradation and loss of capacity.¹³ Tesla has recently proposed a larger format cylindrical 4680 cell, referring to 46 mm in diameter and 80 mm in cylinder height, as measured by the external casing. Larger format cells provide benefits for energy density and power output but potentially exacerbate the internal current and temperature heterogeneity by having a longer jelly-roll. Increasing the cylinder diameter may also prove problematic for effective thermal management due to decreased surface-area-to-volume ratio of the cell. To address these problems, Tesla proposes a “tabless” current collection method¹⁴ by using the current collector foil itself with a contiguous array of current collectors extending from the edge of the foil. This should mean that the current distribution inside the cell is much more uniform with the majority of the edge of each current collector foil being held at the same potential. In theory, this design reduces much of the ohmic loss inside the cell and with it much of the heat produced.

Simulations are presented that utilize the new cell format and different tabbed and tabless current collection designs to demonstrate current heterogeneity and predict temperature resulting under different cooling scenarios. The simulations provide data that is in stark contrast and demonstrates the importance of the ohmic losses to thermal management, even with a modest discharge rate of 1C. The computational framework makes use of underlying physical models, rather than equivalent circuits and should provide valuable insights for battery design and future degradation studies.

Method

A method was previously presented for studying the coupled electrochemical and thermal properties of cylindrical cells using

tomography-based computational domain.⁵ For the interested reader, all model equations, parameter values and solution procedures are presented there. Presently, we generate a larger domain parametrically and introduce continuous tab boundary conditions for the current. The open source software *PyBaMM* is used for the electrochemistry^{15,16} described by porous electrode theory, using the model of Doyle, Fuller and Newman (DFN)^{17,18} and *OpenPNM* is used for the global current and thermal transport.¹⁹ It is assumed that charge transport in the current collectors is one-dimensional along the spiral length, whereas charge transport in the electrodes and separator is one-dimensional in the direction normal to the current collectors (radially). This results in a so-called “1+1D” model that can be solved together iteratively.

Previously, a parameter set was gathered and combined from the literature using: LG MJ1 18650²⁰ for the equilibrium potentials and entropic changes for each electrode (graphite with silicon anode and NMC-811 cathode) and the similar LG M50 21700²¹ cell was used for all other parameters except thermal properties which are taken from Chen et al.²² The same parameter set is used in the present study and so are indicative of how a generic chemistry will behave in a larger format cell.

To make the jelly-roll, a long double-sided electrode “sandwich” is rolled around itself forming a spiral. The model comprises 40 rolled layers and computational nodes are generated at every 10 degrees in the current collector (cc) domains forming a resistor network. For the tabless geometry we assume that the edge of the foil is extended at specific arc angles as depicted in Tesla’s patent¹⁴ (Figs. 6D and 6E) which forms a so-called “shingled spiral.” As the length of each layer steadily increases by tracing the perimeter of the spiral, the length of the extended sections of c.c. also increase. We assume the ratio of the length of the extended to adjacent unextended section is always approximately 2:1. Heat is assumed to be dissipated at the outer boundaries of the cell only. Figure 1 shows the computational domains for each current collector design and the convective heat loss boundary conditions for each case are shown in Table I.

Global heat transfer—model equations.—Heat transport is calculated based on the assumption that the battery is a homogenous medium with volume averaged thermal properties. The energy balance equation can be written as

$$\rho C_p \frac{\partial T}{\partial t} = \nabla(\kappa \nabla T) + Q$$

^zE-mail: t.tranter@ucl.ac.uk; d.brett@ucl.ac.uk

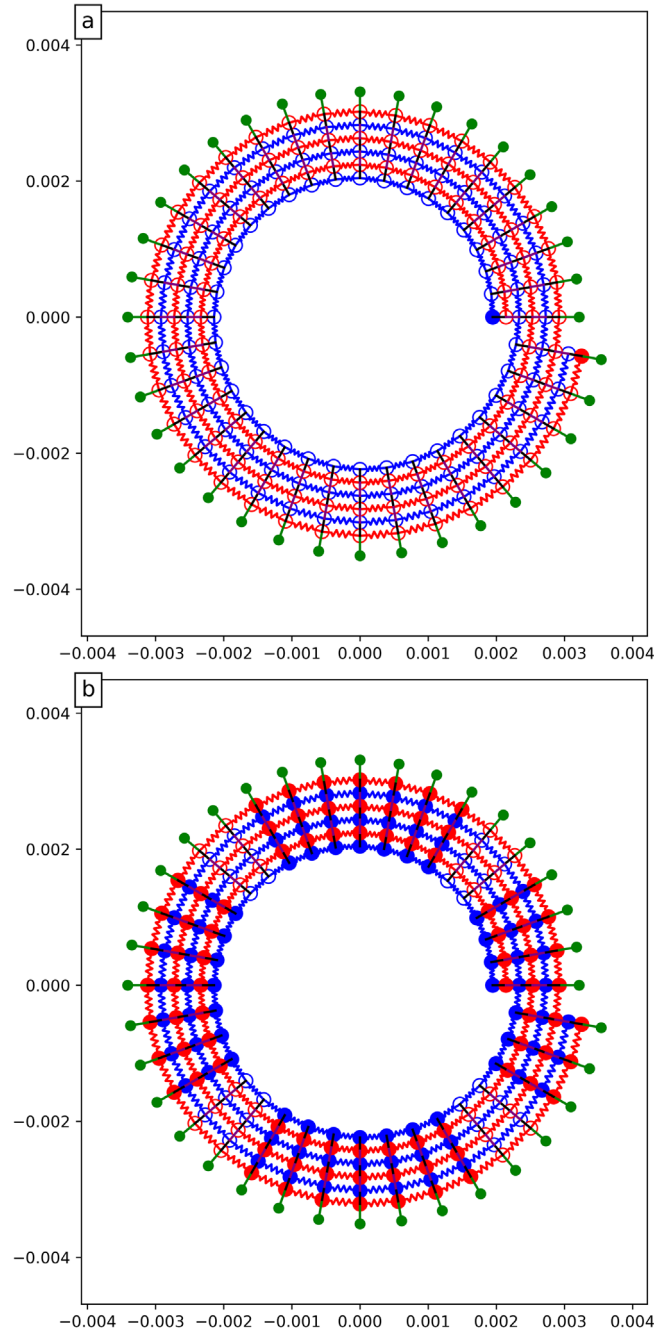


Figure 1. Domains for (a) standard tabs and (b) “tabless” configuration. Three layers are shown instead of 40 for clarity. Current collectors are shown as resistors forming a network around the jellyroll. Empty nodes are junctions in the network and solid nodes are the locations of tabs. Blue represents negative and red positive current collectors and green represents the thermal boundary of the outer casing.

Table I. Cases studied.

Convective heat loss [$\text{W m}^{-2} \text{K}^{-1}$]	Standard tabs	Tabless
10	A	E
28	B	F
50	C	G
100	D	H

where ρ is the density, C_p is the specific heat capacity at constant pressure,

$$\rho = \frac{\sum l_i \rho_i}{\sum l_i}, C_p = \frac{\sum l_i \rho_i C_{p,i}}{\sum l_i \rho_i}$$

κ is the thermal conductivity which is considered to be anisotropic and when divided by the lumped specific heat and densities becomes a thermal diffusivity. Anisotropic thermal conductivity is assumed in the directions parallel and perpendicular to the current collector windings, termed the spiral direction and the radial directions.

$$\alpha_{\text{spiral}} = \frac{\sum l_i}{\sum l_i C_{p,i} \rho_i / \kappa_i}, \alpha_{\text{radial}} = \frac{\sum l_i \kappa_i / C_{p,i} \rho_i}{\sum l_i}$$

Q represents the heat sources generated from the DFN model, which contain an ohmic component and from the ohmic losses in the resistor network:

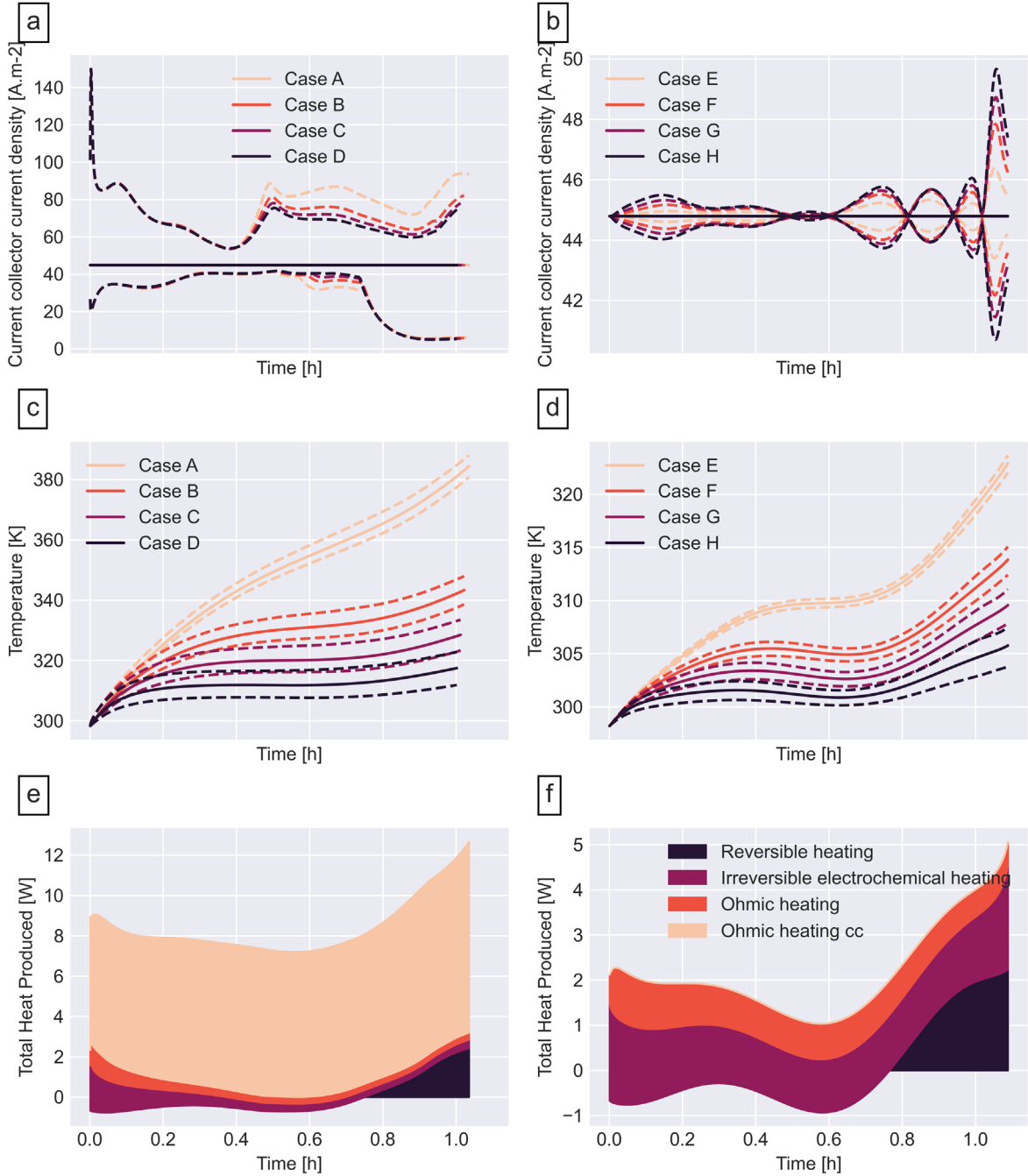


Figure 2. A distribution of current density and temperature occurs within the jellyroll during operations. The plots (a)–(d) show the minimum and maximum values in dashed and the mean values in solid for the cases with different cooling coefficients. Results for standard tabs are on the left and on the right the tabless design. The various contributions to the heat sources for the least cooled cases (cases A and E) are shown for the standard tab design (plot e) and tabless design (plot f). A single discharge is performed and the location of the minimum and maximum current density will shift spatially during the discharge as shown in later snapshot figures.

$$Q = Q_{ohm} + Q_{rxn} + Q_{rev}$$

where

$$Q_{ohm} = -i\nabla\phi, Q_{rxn} = aj\eta, Q_{rev} = ajT\frac{\partial U}{\partial T}$$

where i is the current, ϕ is the potential, a is the surface area to volume ratio of the active material, j is the local current density, η is the overpotential, $\frac{\partial U}{\partial T}$ is the change in open circuit potential with temperature or entropic change. A finite-difference approach is used

to solve the transient heat transport problem utilizing a heat resistor network employing Fourier's Law of conduction¹⁹ with Newton boundary conditions applied to the outer nodes of the jelly-roll and no-flux thermal boundary condition on the inner layer.

Results and Discussion

Figure 2 shows the variation in local current density and temperature for all the cases and heat output for the least cooled cases. Discharging the cell at an approximate rate of 1C (17.5 A) with the conventional tab design results in very wide distributions of local current density due to the high ohmic losses around the length

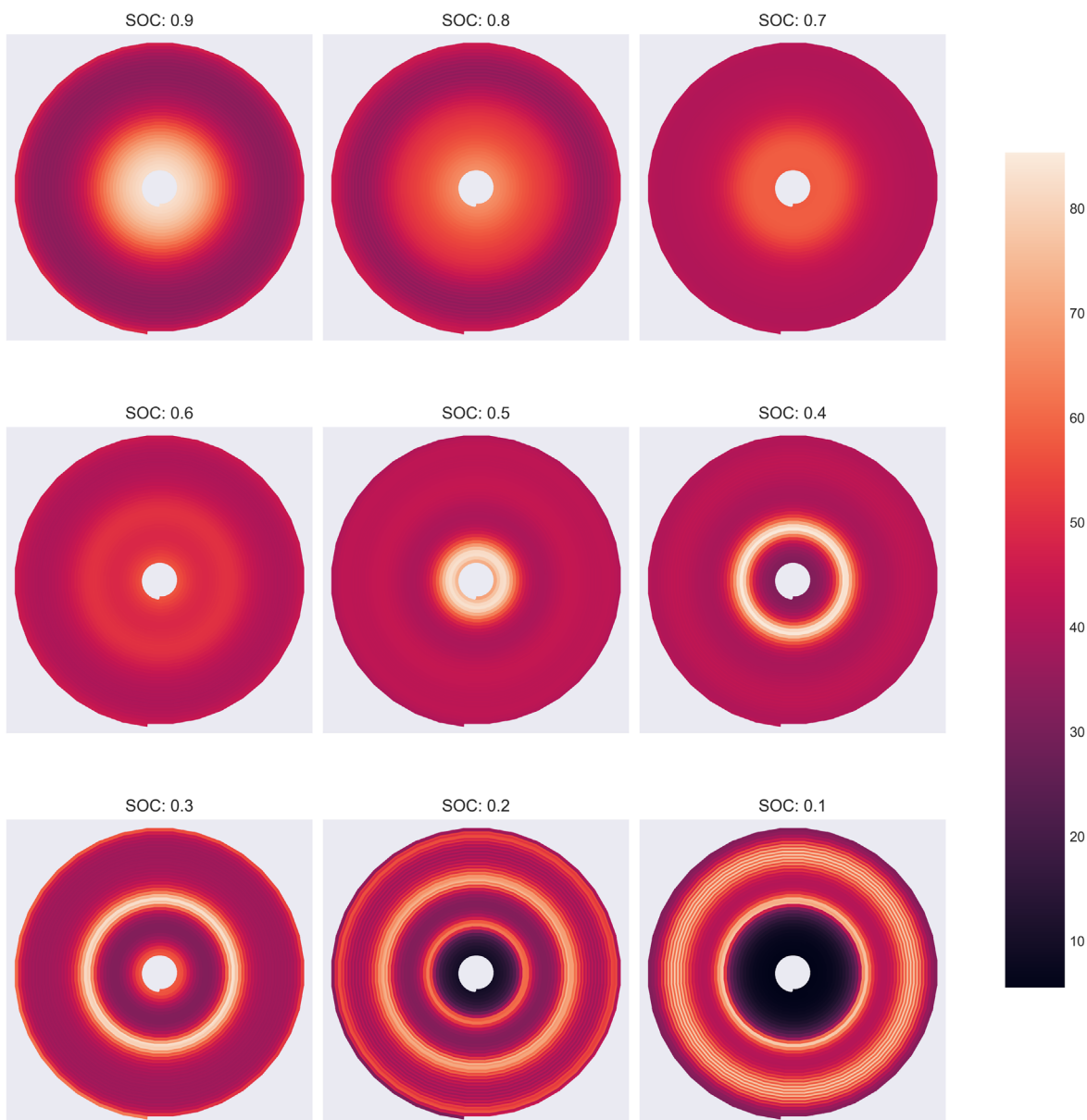


Figure 3. Current density snapshots at various states-of-charge for Case A. Local regions of high intensity are particularly visible after discharging to 0.5 SOC.

of the current collectors. The C-rate is approximate because the simulations were terminated at a specific cut-off voltage (2.7 V) and this was reached earlier for the tabbed cases. There is also some temperature dependence on the cell voltage with higher temperatures allowing the cell to run for slightly longer. The high ohmic loss in the current collectors produces large amounts of heat which can be seen in Fig. 2e. If the cell is not actively cooled this leads to more than 80 degrees in temperature rise above ambient in the worst-case scenario with minimal loss of heat to the environment. The temperature increase and gradients are confirmed with a simple steady-state analysis provided as (supplementary information is available online at stacks.iop.org/JES/167/160544/mmedia). Higher C-rates would lead to even greater temperatures, as would charging the cell where the reversible heat contribution becomes mostly exothermic. Conversely, using Tesla's proposed tabless design results in much more homogenous local current density and reduced ohmic losses along the length of the current collectors. This leads to only a 20 degree rise above ambient, some 60 degrees less than with the traditional tab design.

This difference is attributed almost entirely to the ohmic heating in the current collectors which are negligible for the tabless cases and can hardly be seen in Fig. 2f. Increasing the thickness of the current collector foils would also improve the ohmic heating for the traditional tab design as discussed in the supplementary information.

Figures 3 and 4 show snapshots of the instantaneous local current density at different stages of the discharge for the cases with no active cooling and different tab designs (A & E). With the traditional tabs (Case A above) very localised hotspots can be observed and a much larger range in current density, whereas the tabless design provides a much more even distribution. The hot-spots appear as rings which move gradually in a wave-like fashion, expanding like ripples. These wave-like changes can be explained by the internal local resistance changing at relatively different rates for different sections as they discharge unevenly, as explained previously.⁵ It is expected that local current hot-spots would lead to higher rates of degradation which could be exacerbated further by higher frequency cycling around a fixed state-of-charge.

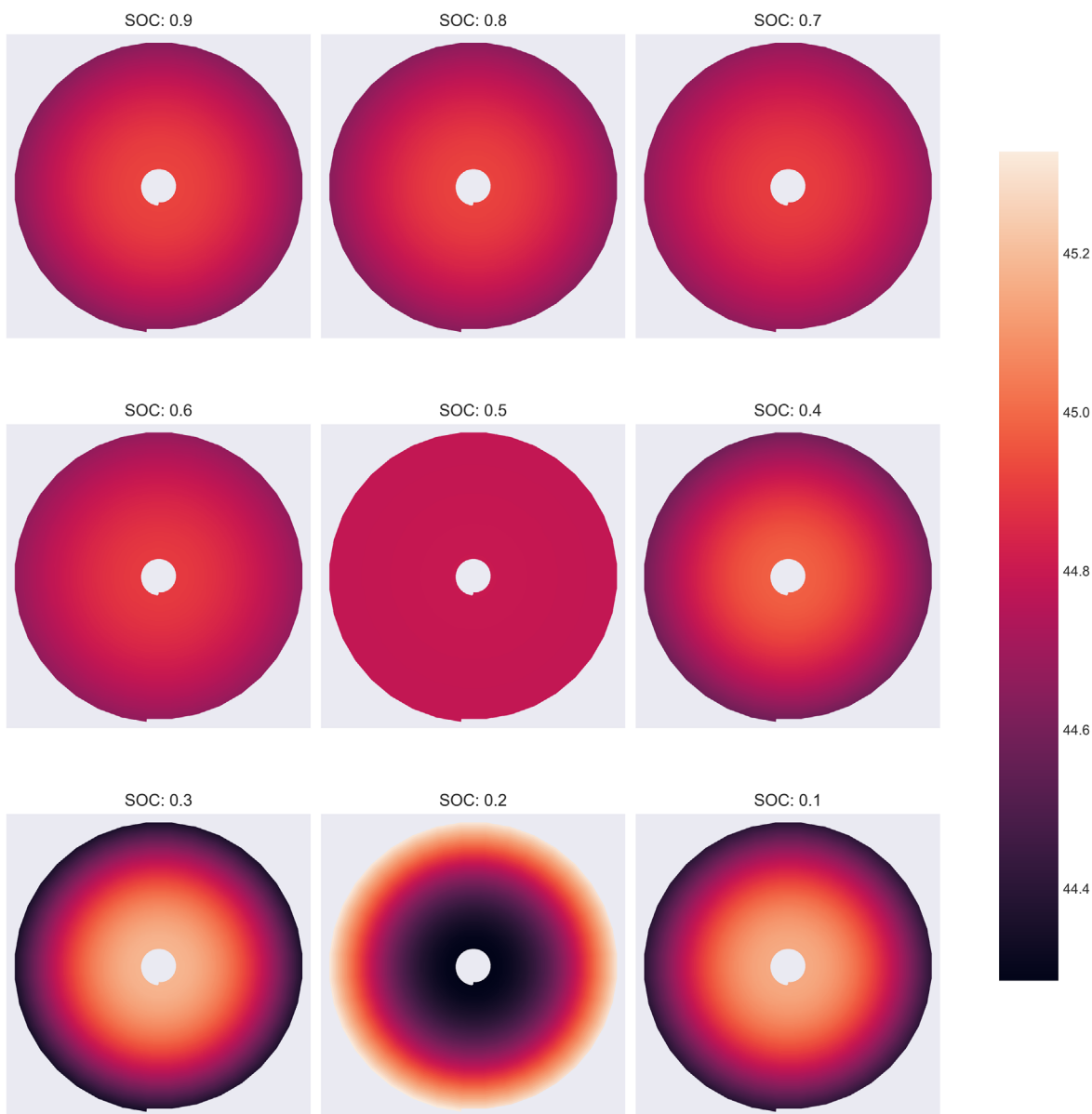


Figure 4. Current density snapshots at various states-of-charge for Case E. A much more homogenous distribution is observed compared to the cases with standard tabs.

Conclusions

A coupled methodology for solving electrochemistry and thermal transport is applied to an idealized spiral geometry representing the new 4680 cylindrical cell. As before, wave-like variations in local current density are observed and are attributed to the local equivalent resistance changes in the battery electrode sections. With the larger cell format, the heterogeneity in current collection resulting from high ohmic losses along the length of the jelly-roll are exacerbated and must be addressed by the tabless design. When using the traditional end-tab design, the ohmic losses from the current collectors results in five times more energy being lost as waste heat, compared with the tabless case.

By observing the results of the simulations, the benefits of going tabless are clear. However, the connections between foil edges and casings are not included in the model and will be a factor in determining manufacturing complication and internal resistance. Future work should include these effects. The modelling framework may also be extended to include 3D profiles along the cylinder height so that different cooling strategies, such as base-plate cooling, can be included.

Acknowledgments

The authors would like to thank Dr. Jacqueline Edge for her management of the Faraday Institution Multiscale Modelling project which provided funding and support under grant number EP/S003053/1, FIRG003 and all members of the project for their useful discussions. TGT would also like to thank all contributors to the PyBaMM and OpenPNM open source software projects. PRS acknowledges The Royal Academy of Engineering (CiET1718/59).

ORCID

T. G. Tranter <https://orcid.org/0000-0003-4721-5941>
 R. Timms <https://orcid.org/0000-0002-8858-4818>
 P. R. Shearing <https://orcid.org/0000-0002-1387-9531>
 D. J. L. Brett <https://orcid.org/0000-0002-8545-3126>

References

1. Q. Wang, B. Jiang, B. Li, and Y. Yan, *Renew. Sustain. Energy Rev.*, **64**, 106 (2016).
2. K. Shah, V. Vishwakarma, and A. Jain, *J. Electrochem. Energy Convers. Storage*, **13**, 030801 (2016).

3. Y. Troxler, B. Wu, M. Marinescu, V. Yufit, Y. Patel, A. J. Marquis, N. P. Brandon, and G. J. Offer, *J. Power Sources*, **247**, 1018 (2014).
4. J. B. Robinson, P. R. Shearing, and D. J. L. Brett, *J. Imaging*, **2**, 2 (2016).
5. T. G. Tranter et al., *J. Electrochem. Soc.*, **167**, 110538 (2020).
6. K. Somasundaram, E. Birgersson, and A. S. Mujumdar, *J. Power Sources*, **203**, 84 (2012).
7. S. C. Chen, Y. Y. Wang, and C. C. Wan, *J. Electrochem. Soc.*, **153**, A637 (2006).
8. D. H. Jeon and S. M. Baek, *Energy Convers. Manag.*, **52**, 2973 (2011).
9. C. Bolsinger and K. P. Birke, *J. Energy Storage*, **21**, 222 (2019).
10. B. Wu, V. Yufit, M. Marinescu, G. J. Offer, R. F. Martinez-Botas, and N. P. Brandon, *J. Power Sources*, **243**, 544 (2013).
11. T. D. Hatchard, D. D. MacNeil, A. Basu, and J. R. Dahn, *J. Electrochem. Soc.*, **148**, A755 (2002).
12. C. Forgez, D. Vinh Do, G. Friedrich, M. Morcrette, and C. Delacourt, *J. Power Sources*, **195**, 2961 (2010).
13. M. D. R. Kok, J. B. Robinson, J. S. Weaving, A. Jnawali, M. Pham, F. Iacoviello, D. J. L. Brett, and P. R. Shearing, *Sustain. Energy Fuels*, **3**, 2972 (2019).
14. K. Tsuruta, M. E. Dermer, and R. Dhiman, "Cell with a tabless electrode." *U.S Patent Application No.*, **US16**, 673,464 (2020), <https://patents.google.com/patent/US20200144676A1/en>.
15. V. Sulzer, S. Marquis, R. Timms, M. Robinson, and S. J. Chapman, "Python Battery Mathematical Modelling (PyBaMM)." *ECSSarXiv Preprints*, **1**, 1 (2020).
16. S. G. Marquis, V. Sulzer, R. Timms, C. P. Please, and S. J. Chapman, *J. Electrochem. Soc.*, **166**, A3693 (2019).
17. M. Doyle, T. F. Fuller, and J. Newman, *J. Electrochem. Soc.*, **140**, 1526 (1993).
18. T. F. Fuller, M. Doyle, and J. Newman, *J. Electrochem. Soc.*, **141**, 1 (1994).
19. J. Gostick et al., *Comput. Sci. Eng.*, **18**, 60 (2016).
20. J. Sturm, A. Rheinfeld, I. Zilberman, F. B. Spingler, S. Kosch, F. Frie, and A. Jossen, *J. Power Sources*, **412**, 204 (2019).
21. C.-H. Chen, F. Brosa Planella, K. O'Regan, D. Gastol, W. D. Widanage, and E. Kendrick, *J. Electrochem. Soc.*, **167**, 080534 (2020).
22. S. C. Chen, C. C. Wan, and Y. Y. Wang, *J. Power Sources*, **140**, 111 (2005).